Structural, magnetic and magnetocaloric properties of (Pr,Sm)2Fe17 compound at room temperature

H. Jaballah, W. Bouzidi, R. Fersi, N. Mliki, Lotfi Bessais

Version of Record: https://www.sciencedirect.com/science/article/pii/S0022369721005047
Manuscript_f9981852aa018defffcfbea00c658448

Structural, magnetic and magnetocaloric properties of $(Pr,Sm)_2Fe_{17}$ compound at room temperature.

H. Jaballah,[1,2] W. Bouzidi,[2] R. Fersi,[1] N. Mliki,[1] and L. Bessais[2]

[1] *Université de Tunis El Manar, Faculté des Sciences de Tunis, Laboratoire Matériaux Organisation et Propriétés, Tunis 2092, Tunisia.*

[2] *Univ Paris Est Creteil, CNRS, ICMPE, UMR 7182, 2 rue Henri Dunant, F-94320 Thiais, France*

(Dated: October 5, 2021)

In the present work, we report on the structural, magnetic, and magnetocaloric properties of the $(Pr, Sm)_2Fe_{17}$ system prepared by arc melting under high pure argon and homogenized at 1073 K to minimize other possible impurity phases. X-ray diffraction (XRD) coupled with Rietveld analysis with FullProf computer code reveals the presence of a single-phase of $(Pr, Sm)_2Fe_{17}$. This compound crystallizes in the rhombohedral Th_2Zn_{17} type structure. The lattice parameters decrease when Sm substitutes Pr. Hence, the temperature dependence of the magnetization is determined. The Curie temperature increases from 285 K to 299 K after the Pr substitution. This increase in T_C is mainly due to the de Gennes factor. The Arrott plot around second-order magnetic transition, magnetic entropy changes ΔS_M, the relative cooling power, and temperature-averaged entropy change (TEC) are reported. This compound is considered a magnetic refrigerant for use at a low magnetic field based on these results.

PACS numbers: 75.50.Bb, 75.50.Tt, 76.80.+y
Keywords: Intermetallic rare-earth transition-metal compounds; Magnetic materials; Magnetocaloric Effect.

I. INTRODUCTION

The R-M intermetallic compounds combining a rare earth element (R) and a transition metal (M) have interesting properties due to their extremely varied potential applications. Among these applications, we may cite the high-density magnetic recording $Sm_2Co_{17}-Cu$ [1], and TbFeCo [2], the hard magnetic materials SmCo, NdFeB, and PrCo [3–6], and the magnetic refrigeration [7].

Iron-rich R_2Fe_{17} intermetallic compounds are studied in several works for their: magnetic properties, as well as their thermodynamic properties, and the absence of thermal hysteresis [8–19]. Additionally, Kou *et al.* [20] have analyzed the magnetic anisotropy in several R_2Fe_{17} systems, where R = Ce, Pr, Nd, Sm, Gd, Tb, Dy, Ho, Er, Tm, Lu, Y. Moreover, absorption and storage capacity of hydrogen were examined by Isnard *et al.* in R_2Fe_{17} (R = Ce, Pr, Nd, Gd) [21]. Their magnetostriction and thermal expansion properties were also studied by Mori *et al.* [22]. Sun *et al.* [23] have reviewed the magnetic properties, Fe-Fe and R-Fe exchange interactions for R_2Fe_{17} and their nitrides. Also, Long *et al.* [24] have as well investigated neutron and Mössbauer effect of Pr_2Fe_{17} and $Pr_2Fe_{17}N_{2.6}$. Further information about structural, magnetic, and microscopic physical properties of Sm_2Fe_{17} and Pr_2Fe_{17} and their nitrides have been provided by Zeng *et al.* [25].

On the other hand, for many years, human activities have led to a sharp increase in greenhouse gas emissions due to the need for refrigeration, air conditioning, and cryogenics. However, these systems mostly use refrigerants that contain volatile organic compounds such as hydrofluorocarbons. Such compounds are made up of carbon and hydrogen, which can easily be found in gaseous form in the atmosphere and cause climatic damages. They can also have harmful effects on animals and plant species as well as on humans. Thus, using less polluting refrigeration systems becomes crucial in this situation.

Magnetic refrigeration is an alternative way for cooling matter using a magnetic field. In the last years, a reasonable interest has been giving to the study of magnetocaloric materials. [10, 26–32]. Many research studies have reported materials with high magnetocaloric effect (MCE) at high temperatures, but few have interesting MCE and second-order magnetic transitions around 300 K. Since discovering MCE, the researchers have studied several magnetocaloric materials; the most promising materials for magnetic refrigeration at room temperature are $Gd_5(Ge,Si)_4$ [27, 33–35], $La(Fe,Co,Si)_{13}(H,C)$ [36–41], Fe_2P [42–45], manganites $R_{1-x}A_xMnO_3$ [46–49] and related alloys and compounds.

Gadolinium is the only element having a high magnetocaloric effect near room temperature. However, its relatively rapid oxidation corrosion, high price, and insufficient global resources do not allow it to compete with conventional refrigeration systems. This work aims to synthesize new material with an interesting magnetocaloric effect room temperature, chemically stable, and lower costs than Gd. We focus on iron-rich Pr_2Fe_{17} based compounds, its relatively large magnetic entropy change maximum around room temperature with a large full width at half-maximum of magnetic entropy change and its reversible magnetocaloric effect make Pr_2Fe_{17} a good competitor for Gd-based magnetic materials. Nevertheless, its Curie temperature (the working temperature in materials for cooling application) is lower than room temperature. To obtain a Curie temperature equal to room temperature is possible to substitute the Pr atom with Sm atom because the Curie temperature of

Sm_2Fe_{17} is higher than room temperature. Several samples $(Pr,Sm)_2Fe_{17}$ have been prepared with different compositions (x=0.24, x=0.3, x=0.36 and x=0.42), only the composition with the nominal composition x=0.36 one gives T_C= 300 K. Here, we present the structural, magnetic, and magnetocaloric properties of (Pr, Sm)$_2$Fe$_{17}$ with the nominal composition x=0.36.

II. EXPERIMENTAL METHODS

(Pr, Sm)$_2$Fe$_{17}$ with the nominal composition x=0.36 has been prepared from high pure elements iron(Fe) 99.9%, praseodymium (Pr) 99.98% and samarium(Sm) 99.98% by arc-melting technique under a purified argon atmosphere. The elements are placed in a copper crucible cooled by cold water. After ingot formation, the compound is wrapped in tantalum foil and introduced into a silica tube sealed under secondary vacuum 2×10^{-6} bar [50–52]. The ingot has been heat-treated for seven days at 1073 K, and is finally water quenched [53–55].

Phase analysis has been performed by X-ray powder diffraction (XRD), using D8 Brucker diffractometer with Cu Kα radiation $\lambda = 1.54178$ Å. XRD data of the samples have been collected between 20° and 80° at room temperature with 0.015 step width.

XRD diagrams are analyzed with the Rietveld method [56, 57] using the Fullprof program [58, 59]. The peak shape function has been selected as Thompson-Cox-Hastings pseudo-Voigt type [60]. The goodness of fit indicators R_B and χ^2 are calculated from the program output to measure the quality of refinement, and they are defined as:

$$R_B = 100 \frac{\sum_K |I_K(O) - I_K(C)|}{\sum_K I_K(O)}$$

and

$$\chi^2 = \frac{\sum_i w_i |y_i(O) - y_i(C)|}{N - P}$$

where $I_K(O)$ is the observed Bragg intensity and $I_K(C)$ is the calculated one. $y_i(O)$ is the intensity observed at the i^{th} step in the step scanned powder diffraction pattern, $y_i(C)$ is that calculated, and w_i is the weight of the observation. N is the total number of points used in the refinement, and P is the number of refined parameters.

The refined parameters are unit cell parameters, scale factors U, V, W, background points, and atomic positions [5, 61–63]. The atomic input parameters that have been used to determine the structure of our samples are from Ref. [9, 64, 65]

Magnetic properties are measured using a magneto/susceptometer Manics DSM8 operating on the same principle as a Faraday type balance between 300 and 900 K [66]. A Physical Properties Measurement System (PPMS) magnetometer is used for magnetic measurements at low temperatures between 200 and 340 K. Recently, it has been reported that the demagnetizing field might have a notable influence on the result of magnetocaloric effect [67]. To get the internal field H_{int}=H_{ext}-N_{Demag}M(T, H_{ext}), where M is the measured magnetization, the external applied magnetic field H_{ext} has been corrected for the demagnetization effect. Demagnetization constant N_{Demag} has been determined from M vs H_{ext} curve in a low field region following the method given in Ref [68]. The corrected magnetic field H_i has been used for the present magnetic results.

III. RESULTS AND DISCUSSION

A. Structure analysis

XRD patterns of the Pr_2Fe_{17} and the $Pr_{1.64}Sm_{0.36}Fe_{17}$ compounds are presented with their Rietveld refinement in Fig. 1(a) and Fig. 1(b), respectively. The pure Pr_2Fe_{17} compound crystallizes in a rhombohedral structure of the Th_2Zn_{17} type in the space group $R\bar{3}m$. In this structure, Pr atoms occupy 6c sites, while Fe atoms occupy four different crystallographic sites: $18f, 18h, 6c$ and $9d$ (in Wyckoff notation).

Table I. a and c unit cell parameters, R_B, χ^2 factors, and atomic positions from Rietveld refinement of $Pr_{2-x}Sm_xFe_{17}$.

	$x = 0$	$x = 0.36$
a (Å)	8.5848 (3)	8.5796 (4)
c (Å)	12.4659 (1)	12.4647 (4)
c/a	1.4521	1.4526
V (Å^3)	795.67	794.63
χ^2	1.45	2.08
R_B	2.98	4.103
$x\{18f\}$(Fe)	0.284	0.283
$x\{18h\}$(Fe)	0.506	0.503
$z\{6c\}$(Pr)	0.345	0.356
$x\{6c\}$(Fe)	0.093	0.092
$z\{18h\}$(Fe)	0.157	0.166

The Rietveld refinement shows that the $Pr_{1.64}Sm_{0.36}Fe_{17}$ compound crystallizes in the same space group as Pr_2Fe_{17} ($R\bar{3}m$). The atomic, strctural parameters, R_B and χ^2 factors are listed in Table I.

Fig. 2 shows that after the partial substitution of Pr by Sm, we notice a small decrease in the lattice parameters a, c and V. For $x = 0$, a and c are respectively 8.5848(3) and 12.4659(1) Å . Similar lattice parameter values and atom positions were found in the previous work [9, 64]. For $x = 0.36$ a and c are 8.5796(4) and 12.4647(4) Å,

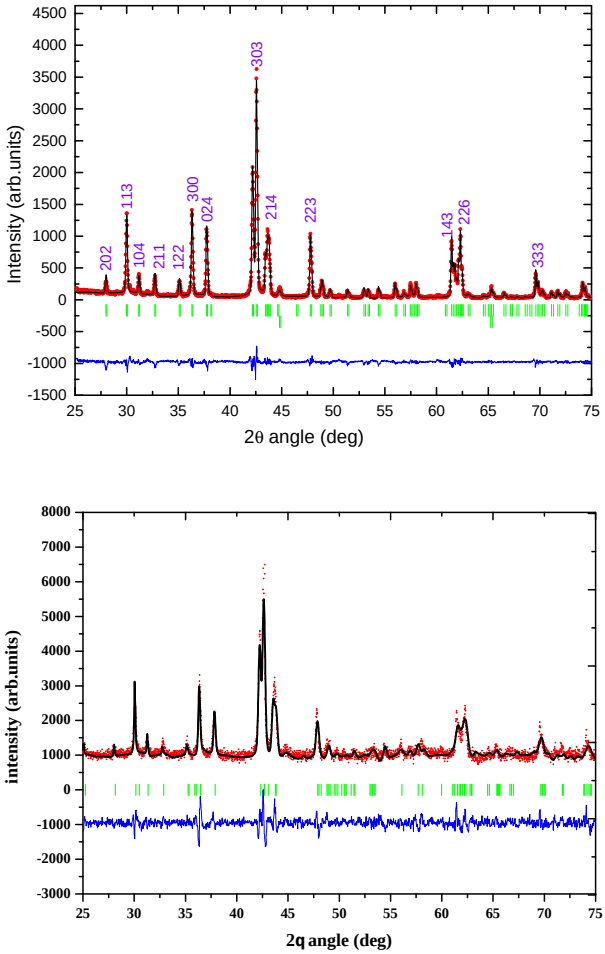

Figure 1. The Rietveld refinement pattern of XRD data for (a) Pr_2Fe_{17} and (b) $Pr_{1.64}Sm_{0.36}Fe_{17}$ compounds. The black and red line presents respectively the calculated intensities and the experimental intensities. The green vertical bars correspond to (hkl) line positions (Positions of Bragg peaks). The blue line shows the difference between the calculated and experimental intensities.

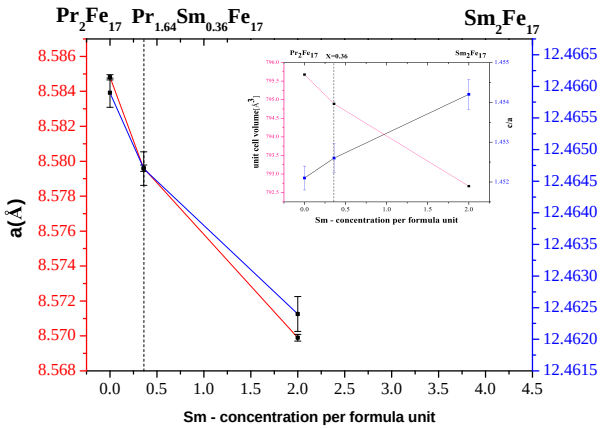

Figure 2. Cell parameters versus Sm content x, Inset shows cell volume and c/a vs Sm content.

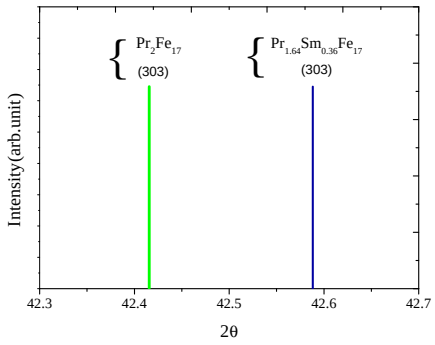

Figure 3. (303) Bragg position for Pr_2Fe_{17}, $Pr_{1.64}Sm_{0.36}Fe_{17}$.

respectively, while slight decrease in cell volume from 795.67 Å^3 to 794.63 Å^3 and c/a ratio remains almost constant. This behaviour can be explained by the size of the Sm atom, which is slightly small compared to the size of the praseodymium one.

For Sm concentration 0 and 0.36, we note that all angular positions shift to the right, in Fig. 3 we show angular position shift of the peak that corresponds to (hkl)≡(303), a decrease of lattice parameters causes the observed shift, several works reported the same behaviour, we can cite Ref. [69]. In order to estimate the concentration of the prepared sample from the outputs of Rietveld refinement, we use Vegard's law; this law has mainly been used in the calculation of solid solution compositions and even recently [69, 70], the simplest expression of this law for a binary (A-B) compound is defined as follows [71]:

$$a_{A-B} = a_A(1-x) + a_B$$

Where a_{A-B}, a_A, a_B are lattice parameters of binary compound, pure A compound and pure B compound, respectively. From a value of Pr_2Fe_{17}, Pr_{2-x} Sm_xFe_{17} and Sm_2Fe_{17} the preceding equation gave $x \sim 0.35$ which is very close to the nominal composition within the experimental uncertainties.

B. Magnetic properties

Here, we present the magnetic properties of $Pr_{1.64}Sm_{0.36}Fe_{17}$ compound. It is worthy to note that this composition has been chosen for the following reason: It is well known that T_C of Pr_2Fe_{17} and Sm_2Fe_{17} are equals to 285 and 386 K, respectively. To obtain a compound with a Curie temperature around the room temperature, we started by preparing Pr_2Fe_{17} as the initial mixture, and we used the nearly linear variation of

$Pr_{2-x}Sm_xFe_{17}$ Curie temperature with Sm content to reach $T_C \sim 300\,K$. Therefore, for $x = 0.36$, this goal is achieved.

Magnetization variation as a function of the temperature is measured under a weak magnetic field equal to 0.05 T. The Curie temperature T_C is determined by calculating the first derivative of $M(T)$. The value of the Curie temperature corresponds to the minimum of the magnetization derivative curve. We notice that T_C increases after the substitution of the Pr atom by the Sm atom.

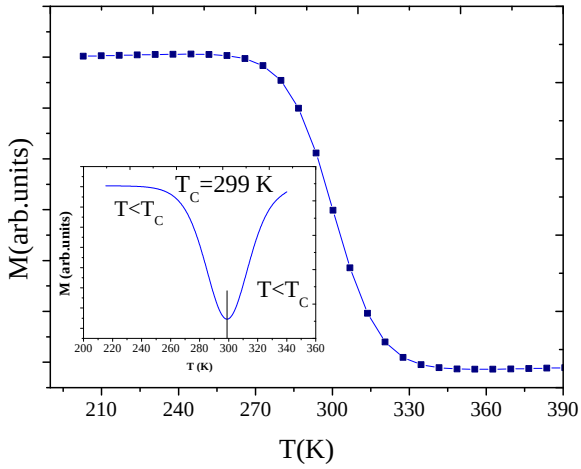

Figure 4. Temperature dependence of magnetization of $Pr_{1.64}Sm_{0.36}Fe_{17}$ under an applied magnetic field $\mu_0 H = 0.05\,T$.

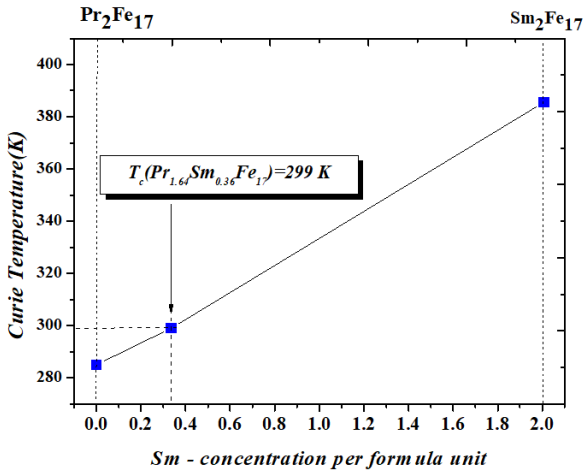

Figure 5. T_C versus Sm content (x) of $Pr_{2-x}Sm_xFe_{17}$ compounds

Fig. 4 shows the variation of the magnetization as a function of the temperature. It shows a sudden drop in magnetization, the signature of a phase transition from a ferromagnetic state to a paramagnetic one. The value of T_C for the compound Pr_2Fe_{17} is equal to 285 K, this value is consistent with the one found by Gorria *et al.* [13]. After the partial substitution of Pr by Sm T_C increases, it equals 299 K. Fig. 5 shows a quasi-linear variation of T_C with Sm content which is in a good agreement with Vegard's law mentioned above, similar behavior has been reported in [65, 72].

Table II. Interatomic distances ($d_{\text{Fe-Fe}}(\AA)$) and coupling type for the rhombohedral $R\bar{3}m$ structure type for $Pr_{2-x}Sm_xFe_{17}$, $x = 0$ and $x = 0.36$. NN is the number of near neighbor atom.

Sites		$x = 0$	$x = 0.36$	NN
$6c - 6c$	AFM	2.31	2.28	1
$6c - 9d$	FM	2.64	2.637	3
$6c - 18f$	FM	2.69	2.677	6
$6c - 18h$	FM	2.68	2.6	3
$9d - 18f$	AFM	2.43	2.42	2
$9d - 18h$	AFM	2.43	2.4	4
$9d - 6c$	FM	2.63	2.63	4
$18f - 18f$	AFM	2.43	2.42	2
$18f - 18h$	AFM	2.55	2.4	2
$18f - 6c$	FM	2.69	2.68	1
$18h - 9d$	AFM	2.43	2.4	3
$18h - 18h$	FM	2.48	2.5	1
$18h - 6c$	FM	2.67	2.6	2
$18h - 9d$	AFM	2.44	2.4	2
$18h - 18f$	AFM	2.56	2.4	2

T_C in rare-earth transition-metal intermetallic compounds are governed by three kinds of exchange coupling J_{RR}, J_{TT} and J_{RT}. Therefore, T_C can be given by the following relation [73]: which allows us to discuss the different parameters which influence the value of T_C:

$$3k_BT_C = a_{\text{FeFe}} + a_{\text{RR}} + [(a_{\text{FeFe}} - a_{\text{RR}})^2 + 4a_{\text{RFe}}a_{\text{FeR}}]^{1/2}$$

Where $a_{\alpha-\beta}$ is the magnetic interaction energy between α and β spin.

Neglecting the exchange interaction between two rare-earth atoms a_{RR} is relatively weak compared to the other terms of energy of magnetic interaction. So, it can be written as follows:

$$3k_BT_C = a_{\text{FeFe}} + [a^2_{\text{FeFe}} + 4a_{\text{RFe}}a_{\text{FeR}}]^{1/2}$$

Where

$$a_{\text{FeFe}} = Z_{\text{FeFe}}J_{\text{FeFe}}S_{\text{Fe}}(S_{\text{Fe}} + 1)$$

$$a_{\text{RFe}}a_{\text{FeR}} = Z_1Z_2S_{\text{Fe}}(S_{\text{Fe}} + 1)GJ^2_{\text{RFe}}$$

where G is the de Gennes factor:

$$G = (g_{\text{R}} - 1)^2J_{\text{R}}(J_{\text{R}} + 1)$$

J_{FeFe} and J_{RFe} are the exchange coupling constant between tow iron atoms and between iron atom and rare-earth atom, respectively.

g_{R} is the Landé factor of rare-earth atom.

S_{Fe} and J_{R} are the spin moment of the iron atom and the total moment of rare-earth atom, respectively.

In $Pr_{1.64}Sm_{0.36}Fe_{17}$, each atom of Pr or Sm has an average of $Z_1 = 19$ iron near-neighbours; each an atom of iron has an average of $Z_2 = 2$ atoms of Pr or Sm and a number of $Z_{\mathrm{FeFe}} = 10$ iron neighbors. This relation shows that T_C is governed by the $3d-3d$ exchange interactions between the transition metal atoms and the $3d-4f$ exchange interactions between the rare-earth and the transition metal. Consequently, T_C is mainly controlled by the exchange interaction between the atoms of iron J_{FeFe} and between the rare-earth atom and the iron atom J_{RFe} [52, 74]. Many parameters can have an influence on the value of T_C in R_2Fe_{17} intermetallic materials. Among these, we can mention de Gennes's factor. Indeed, T_C is governed by the magnetic energies of exchange a_{Fe-Fe} and a_{R-Fe}, the strength of a_{R-Fe} is proportional to de Gennes factor of rare-earth [75–77]. Ref [23] shows the dependence of T_C on the de Gennes factor in R_2Fe_{17} compounds (R = Ce, Pr, Nd, Sm, Gd, Tb, Dy, Ho, Er, Tm). A maximum of T_C is shown for Gd with the highest de Gennes factor, T_C increases almost linearly when the de Gennes factor increases with different slopes for light and heavy rare-earth atom. Table III shows de Gennes factor values tabulated by Kirchmayr and Poldy (1978)[78]

Figure 6. Curie temperature of R_2Fe_{17} for different rare-earth atom

Table III. de Gennes factor value of different rare earth

$4f^n$	3^+ion	G
1	Ce	0.18
2	Pr	0.80
3	Nd	1.84
5	Sm	4.46
7	Gd	15.75
8	Tb	10.5
9	Dy	7.08
10	Ho	4.5
11	Er	2.55
12	Tm	1.17

Another parameter is affecting T_C in R_2Fe_{17} compounds which is the distances between the iron atoms. In fact, the sign of the exchange integrals is determined by the distances d_{FeFe}, when d_{FeFe} is less than 2.45 Å J_{FeFe} is negative and the coupling between the pair of iron atoms is antiferromagnetic [79]. Otherwise, d_{FeFe} is greater than 2.45 Å the exchange integral becomes positive, and the iron pairs become ferromagnetically coupled. The presence of Fe-Fe distances less than and greater than 2.45 Å in Pr_2Fe_{17} and $Pr_{1.64}Sm_{0.36}Fe_{17}$ compounds results in a competition between two types of ferromagnetic and antiferromagnetic couplings (Table II). The coexistence of a negative and positive coupling is the origin of the relatively low temperature in the compounds Pr_2Fe_{17} and $Pr_{1.64}Sm_{0.36}Fe_{17}$. After the partial substitution of Pr by Sm in Pr_2Fe_{17} the coupling nature of the different pairs of Fe is not affected, but we notice a slight decrease in the Fe-Fe distances in the $6c-6c$ site, which can decrease the value of Curie temperature. So the increase of T_C cannot be explained by the variation of the Fe-Fe distances. Ultimately, there is a competition between the two contributions to T_C: de Gennes factor and iron-iron distance. In Sm_2Fe_{17} compound T_C is equal to 400 K but in Pr_2Fe_{17} T_C is equal to 285 K, although the unit cell volume and iron pairs distance for these two compounds is very close ($V_{Pr_2Fe_{17}} - V_{Sm_2Fe_{17}} = 3\mathring{A}^3$) there is a relatively large difference in the value of T_C. This difference shows that rare-earth-transition metal magnetic energy exchange is much stronger in Sm_2Fe_{17} than in Pr_2Fe_{17}. In conclusion, the contribution of Sm de Gennes factor in magnetic energy exchange can explain the increase of T_C after the partial substitution of Pr by Sm. Similar behavior has been noted for other compounds such as $Pr_{2-x}Dy_xFe_{17}$ [65].

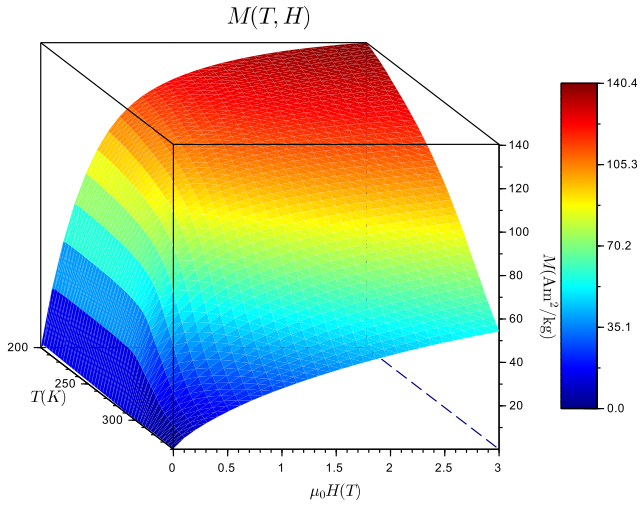

Figure 7. magnetization $M(\mu_0 H, T)$ curves of $Pr_{1.64}Sm_{0.36}Fe_{17}$.

Fig. 7 presents isothermal magnetization $M(\mu_0 H, T)$ measured at different magnetic fields between 0 and 3 T and temperatures from 200 to 340 K. It shows that for temperatures lower than the T_C which corresponds to a ferromagnetic state, the magnetization increases notably according to the magnetic field. However, for temperatures higher than T_C, the material is paramagnetic, the magnetization increases slowly with the applied magnetic field. We also note that for a given magnetic field, the

magnetization decreases when the temperature increases.

Fig. 8 shows the magnetization as a function of the magnetic field applied at the temperature 200 K. To determine the value of the magnetization at saturation and the anisotropy constant we used the following saturation law:

$$M = M_s\left(1 - \frac{a}{H^2}\right)$$

with

$$a = \left(\frac{8}{105}\right)\left(\frac{K}{M_s}\right)^2$$

Where K and M_s are the anisotropy constant and the saturation magnetization, respectively. The anisotropy field can be easily deduced from $H_a = 2K/M_s$. The values of M_s, K and H_a are listed in Table IV.

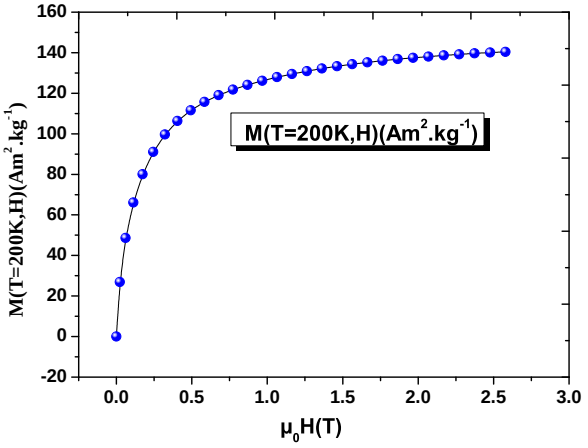

Figure 8. Magnetization $M(H)$ vs magnetic field of $Pr_{1.64}Sm_{0.36}Fe_{17}$ measured at $T = 200$ K .

We plotted the Arrott plots $M^2 = f(H/M)$ deduced from isothermal magnetization $M(H)$ curves (Fig. 9). From the shape and the slope of the curves, we can determine the type of the phase transition: If the slope is negative and the Arrott plots close to the Curie temperature have the S shape, the transition from the ferromagnetic state to the paramagnetic state is, therefore, a first-order transition. If the curves have a single inflexion point and a positive slope, the transition from the ferromagnetic state to the paramagnetic one is a second-order transition.

C. Study of the phase transition according to the Landau model

We develop in this part the Landau model to confirm the nature of the phase transition. The order of the transition phase is determined by developing free magnetic energy as a function of temperature around the T_C,

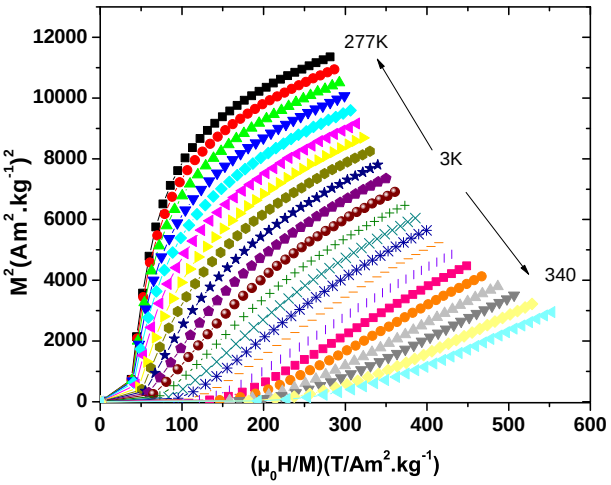

Figure 9. The Arrott plots of $Pr_{1.64}Sm_{0.36}Fe_{17}$ compound.

Table IV. magnetic characterization of $Pr_{2-x}Sm_xFe_{17}$ and Pr_2Fe_{17}

	M_s(Am^{2}kg^{-1})	T_c(K)	K(MJ.m^{-3})	$\mu_0 H_a$(T)
Pr_2Fe_{17}	165	285	5.09	7.33
$Pr_{1.64}Sm_{0.36}Fe_{17}$	146	299	2.49	4.07

neglecting the very high power terms of magnetization. Free energy F as a function of total magnetization can be developed in the form:

$$F = \frac{1}{2}a(T)M^2 + \frac{1}{4}b(T)M^4 + \frac{1}{6}c(T)M^6 - \mu_0 MH$$

Applying the equilibrium condition for free energy

$$\frac{dF}{dM} = 0$$

we obtain:

$$\mu_0 H = a(T)M + b(T)M^3 + c(T)M^5$$

The coefficients $a(T), b(T)$ and $c(T)$ are the Landau parameters determined from the equilibrium condition by plotting $\mu_0 H$ as a function of the magnetization M. $a(T)$ and $c(T)$ are always positive (Fig 10 and Fig. 11), from $a(T)$ we can determine the value of the T_C which corresponds to its minimum. However, $b(T)$ can be positive, zero, or negative, the sign of $b(T)$ can indicate if the magnetic transition is first-order phase transition or second-order phase one (Fig. 12). Indeed, if $b(T_C) \geq 0$ the magnetic transition is a second-order transition phase, otherwise the magnetic transition is a first-order transition phase. For $Pr_{1.64}Sm_{0.34}Fe_{17}$ $b(T_C) \geq 0$ which confirms that the magnetic transition is a second-order type.

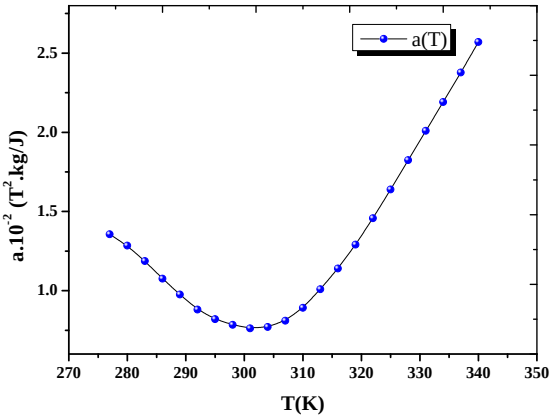

Figure 10. Landau parameter $a(T)$ vs temperature around the T_C for $Pr_{1.64}Sm_{0.36}Fe_{17}$ sample.

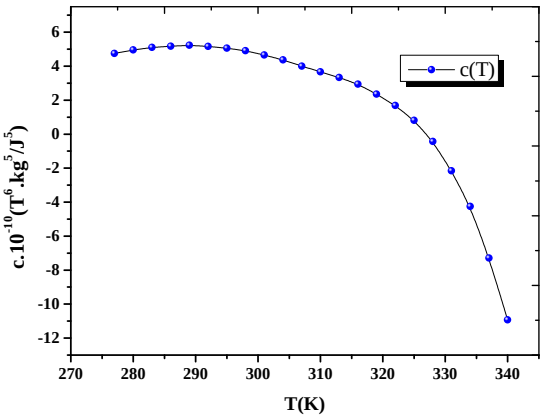

Figure 11. Landau parameter $c(T)$ vs temperature around the T_C for $Pr_{1.64}Sm_{0.36}Fe_{17}$ sample.

D. Magnetocaloric effect

To calculate the variation of the magnetic entropy change caused by the application of a magnetic field, it is necessary to integrate the following Maxwell relation:

$$\Delta S_{\mathrm{M}} = \mu_0 \int_0^H \left(\frac{\partial M}{\partial T}\right)_H dH$$

Where M is the magnetization, T is the temperature, and H is the applied magnetic field. Since, the isothermal $M(H)$ curves are measured by discrete field changes, the following expression might be used [80]:

$$|\Delta S_{\mathrm{M}}| = \mu_0 \sum_i \frac{M_i - M_{i+1}}{T_{i+1} - T_i} \Delta H_i$$

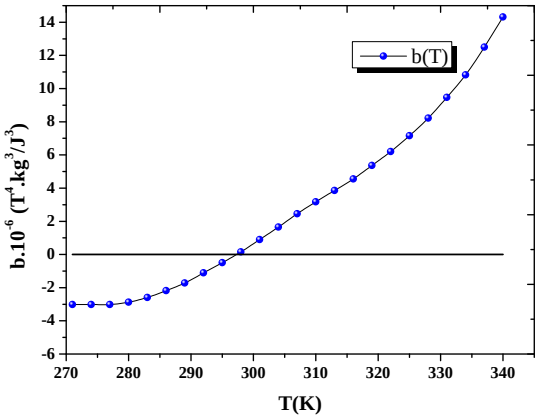

Figure 12. Landau parameter $b(T)$ vs temperature around the T_C for $Pr_{1.64}Sm_{0.36}Fe_{17}$ sample.

Where M_i and M_{i+1} are the initial magnetization at T_i and T_{i+1} temperature respectively when the magnetic field increases by ΔH_i. In table V, we have presents $-\Delta S_{\mathrm{M}}$ values for some R_2Fe_{17} compounds. It clearly shows that $(Pr,Sm)_2Fe_{17}$ has a good magnetocaloric effect at a relatively low field.

Table V. T_C, magnetic entropy change and magnetic field change of some R_2Fe_{17} compounds.

Compound	T_C (K)	$-\Delta S_{\mathrm{M}}$ (J/kgK)	$\mu_0\Delta H$ (T)	Ref
Y_2Fe_{17}	303	3.2	5	[8]
Lu_2Fe_{17}	264	1.5	2	[10]
Nd_2Fe_{17}	339	2.5	1.5	[81]
Nd_2Fe_{17}	331	3.4	1.5	[18]
Gd_2Fe_{17}	475	1.2	1.5	[16]
Pr_2Fe_{17}	286	2	2	[13]
$Pr_{1.64}Sm_{0.36}Fe_{17}$	299	2.5	2	This work
Gd	293	4.8	2	[82]
GdNi	69	9	2	[83]
HoNi	37	6.8	2	[83]
ErNi	10	15	2	[83]
Gd_3Co	128	5	2	[84]
$TbCo_2$	230	4.61	3	[85]
$Gd_5Ge_2Se_2$	275	14	2	[82]

Fig. 13 illustrates the variation of the magnetic entropy around Curie temperature of $Pr_{1.64}Sm_{0.36}Fe_{17}$ for external variation of the magnetic field between 0 and 3 T. For a magnetic field change $\mu_0\Delta H$= 3 T $|\Delta S_{\mathrm{M}}| \sim 3.5$ J/(kg.K) at T= 305 K. The partial substitution of Pr By Sm increase the operating temperature that corresponds to the maximum of $|\Delta S_{\mathrm{M}}|$, is higher in $Pr_{1.64}Sm_{0.36}Fe_{17}$ compared to the parent compound

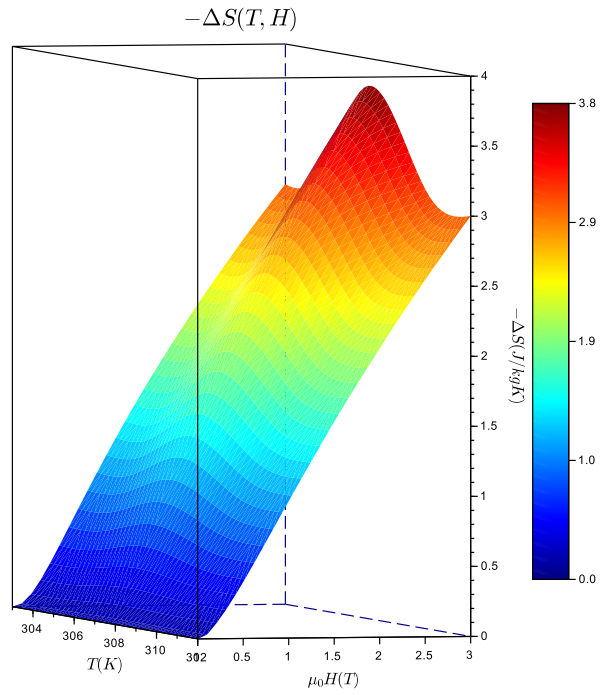

Figure 13. Magnetic entropy change $\Delta S(T,\mu_0 H)_{\rm M}$ for $Pr_{1.64}Sm_{0.36}Fe_{17}$ sample.

Table VI. Magnetocaloric effect of $Pr_{1.64}Sm_{0.36}Fe_{17}$.

$\mu_0\Delta H$(T)	1	1.6	2	2.6	3
$\lvert\Delta S_{\rm M}\rvert$(J/(kg.K))	1.22	1.87	2.5	2.98	3.24
$\delta T^{\rm FWHM}$(K)	51	58	63.76	69.4	78
RCP(J/kg)	62.22	108.46	159.4	202.65	247.26
RC_{Area}(J/kg)	48.46	86.81	121.1	164	195.1

Pr_2Fe_{17}. $|\Delta S_{\rm M}|$ remains almost constant after the substitution with Sm. Even though many research studies have reported materials with high ECM at low temperatures, there are few materials with high MCE and second-order transition phase from ferromagnetic state to paramagnetic state around to 300 K.

The relative cooling power (RCP) is an essential parameter in the magnetocaloric application. It is related with the maximum of entropy change by the following relation [37]:

$$RCP = -\Delta S_{\rm M}\ \delta T^{\rm FWHM}$$

Where $\delta T^{\rm FWHM}$ is the full width at half-maximum in the temperature dependence of the magnetic entropy change, the maximum of $-\Delta S_{\rm M}$, the variation of the temperature ΔT and relative cooling power (RCP) are given in Table VI.

Another important parameter to evaluate the magnetocaloric effect is the refrigerant capacity $(RC)_{\rm Area}$, it is the amount of heat that can be transferred in one thermodynamic cycle. The RC value represents the area under $-\Delta S_{\rm M}$ curve using the temperature of FWHM. It can be calculated by integrating the following expression:

$$RC_{\rm Area}(H) = \int_{T_{min}}^{T_{max}} \Delta S_M(T,H)dT;$$

$$T_{max} - T_{min} = \delta T^{FWHM}$$

In addition to RCP and RC_{area}, temperature-averaged entropy change (TEC) is another parameter that has been used to check the applicability of materials for magnetic refrigeration technologies. TEC was introduced by L. D. Griffith *et al.* [90] as another figure of merit. TEC can be calculated using magnetic entropy change data as follows:

$$TEC = \frac{1}{\Delta T_{H-C}} \max \left\{ \int_{T_{mid}-\frac{\Delta T_{H-C}}{2}}^{T_{mid}+\frac{\Delta T_{H-C}}{2}} |\Delta S_M(T)| dT \right\}$$

Where ΔT_{H-C} is defined as the temperature range for the measuring device and represents the difference between hot and cold heat exchangers. T_{mid} represents the temperature value in the middle of ΔT_{H-C} that maximises TEC. Fig. 14 shows the variation of TEC with ΔT_{H-C} under several magnetic field changes between 1 T and 3 T. One can see that TEC decreases slightly and monotonously with ΔT_{H-C}, it is very close to the maximum of entropy change value for low values of ΔT_{H-C}. It is easy to see that TEC increases monotonically with the applied magnetic field for a given temperature. The obtained TEC(ΔT_{H-C}=5 K, μ_0H=3 T) and TEC(ΔT_{H-C}=5 K, μ_0H=1 T) for $Pr_{1.64}Sm_{0.36}Fe_{17}$ are 3.71 $Jkg^{-1}.K^{-1}$ and 1.4 $Jkg^{-1}.K^{-1}$, respectively. Table VII shows TEC value of our sample and TEC values of other materials for comparison. $Pr_{1.64}Sm_{0.36}Fe_{17}$ $\frac{TEC}{\Delta\mu_0 H}$ is comparable to $\frac{TEC}{\Delta\mu_0 H}$ of $Pr_{0.5}Er_{0.1}Sr_{0.4}MnO_3$ [86] and $TmFe_{0.7}Mn_{0.3}O_3$ [87], slightly higher than $\frac{TEC}{\Delta\mu_0 H}$ of $Pr_{0.5}Eu_{0.1}Sr_{0.4}MnO_3$ [86], $\frac{TEC}{\Delta\mu_0 H}$ of $TmFe_{0.8}Mn_{0.2}O_3$ [87], $\frac{TEC}{\Delta\mu_0 H}$ of $La_{0.8}Na_{0.2}MnO_3$ [88], and $\frac{TEC}{\Delta\mu_0 H}$ of Ho_2CoMnO_6 [89].

RCP for $Pr_{1.64}Sm_{0.36}Fe_{17}$ is around $\sim$ 250 J/kg for a magnetic field change equal to 3 T.

There are several magnetocaloric materials that have been studied for magnetic refrigeration at room temperature: $Gd_5(Ge,Si)_4$ [27, 33–35], La(Fe,Co,Si)$_{13}$(H,C) [36–41], Fe_2P [42–45], manganites $R_{1-x}A_xMnO_3$ [46–49] and related alloys and compounds. In these materials the magnetic transition from the ferromagnetic state to the paramagnetic state is a first order transition phase show a large $|\Delta S_{\rm M}|$ at operating temperature, but possess a low

Table VII. TEC value of our sample and TEC values of other materials for comparison.

Material	T_{mid}	$\Delta\mu_0 H$	ΔT_{H-C}	TEC	$\frac{TEC}{\Delta\mu_0 H}$	Ref
	K	T	K	$J(Kkg)^{-1}$	$J(KkgT)^{-1}$	
$Pr_{1.64}Sm_{0.36}Fe_{17}$	300	3	5	3.71	1.24	This work
$Pr_{0.5}Eu_{0.1}Sr_{0.4}MnO_3$	279.9	5	5	4.45	0.89	[86]
$Pr_{0.5}Eu_{0.1}Sr_{0.4}MnO_3$	188.5	5	5	4.9	0.98	[86]
$TmFe_{0.7}Mn_{0.3}O_3$	11	7	5	7	1	[87]
$TmFe_{0.8}Mn_{0.2}O_3$	12	7	5	6.4	0.914	[87]
$La_{0.8}Na_{0.2}MnO_3$	330	5	5	4.6	0.92	[88]
$La_{0.8}Ca_{0.05}Na_{0.15}MnO_3$	315	5	5	4.55	0.91	[88]
Ho_2CoMnO_6	77	7	5	6.5	0.928	[89]

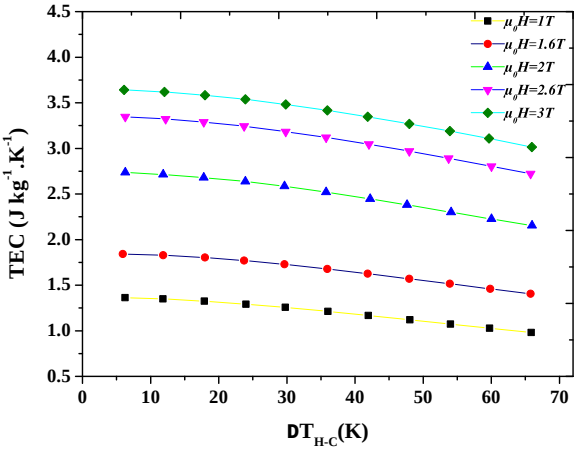

Figure 14. TEC vs ΔT_{H-C} at several magnetic fields for $Pr_{1.64}Sm_{0.36}Fe_{17}$.

RCP because of their low working temperature range $\delta T^{\mathrm{FWHM}} \sim 10\,\mathrm{K}$ as opposed to materials with second order transition phase like the parent compound Pr_2Fe_{17} with $\delta T^{\mathrm{FWHM}} \sim 100\,\mathrm{K}$ [72].

For $Pr_{1.64}Sm_{0.36}Fe_{17}$ *RCP* is found to be around $159.4\,\mathrm{J.kg^{-1}}$ under a magnetic field change of 2 T which is around 75% of that observed in pure Gd and makes our compound a potential candidate for magnetic refrigeration around the room temperature [82].

From the point of view of magnetic refrigeration, the irreversibility of the magnetocaloric effect is a major disadvantage. Indeed, a minimal thermal hysteresis is a basic constraint for a practical refrigerant [91]. For example, the materials mentioned above like $(Gd_5(Ge,Si)_4$, $La(Fe,Co,Si)_{13}(H,C),Fe_2P)$ exhibit a first-order transition phase, show a large $|\Delta S_{\mathrm{M}}|$. However, with a relatively large thermal hysteresis contrary to materials that display a second-order magnetic transition. Compared to these materials, $Pr_{1.64}Sm_{0.36}Fe_{17}$ exhibits a second-order magnetic transition at a T_C very close to room temperature with a moderate $|\Delta S_{\mathrm{M}}|$ and high *RCP*.

It should be mentioned that detailed researches show that the Maxwell relation can not be utilized close to the Curie temperature because of the coexistence of paramagnetic and ferromagnetic phases; the sudden drop in the magnetization causes a discontinuity in the entropy change at Curie temperature. Consequently, the large entropy peak is a fallacious result because of the inappropriate use of the Maxwell relation [92, 93]. For materials that

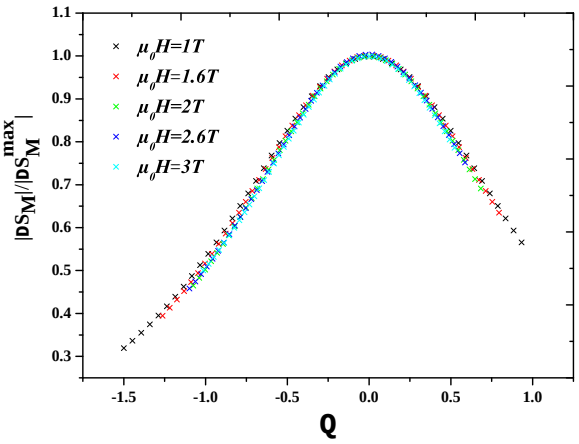

Figure 15. Universal curve of entropy change VS reduced temperature Θ for $Pr_{1.64}Sm_{0.36}Fe_{17}$ sample

.

exhibit a second-order magnetic phase transition from the ferromagnetic to the paramagnetic state, it is possible to obtain a universal phenomenological curve using normalized entropy change $-\Delta S/-\Delta S_{\mathrm{max}}$ as a function of rescaled temperature [94].

$$\Theta = -(T - T_{\mathrm{C}})/(T_{\mathrm{r1}} - T_{\mathrm{C}}), T \leq T_{\mathrm{C}}$$

$$\Theta = (T - T_{\mathrm{C}})/(T_{\mathrm{r2}} - T_{\mathrm{C}}), T \geq T_{\mathrm{C}}$$

Where Θ is the rescaled temperature, Tr1 and Tr2 are the temperatures of the two reference points that have

been selected as those corresponding to $-\Delta S_{\rm M}$=$-a\times$ $\Delta S_{\rm max}$ (where $0 \leq a \leq 1$) [95]. Some theoretical studies have proved that it is not necessary to use two reference point temperatures lower and higher than T_C Tr1 and Tr2, but only one Tr can be used for a material with a single magnetic phase. Nevertheless, in the case of an important demagnetization factor or the existence of multiple magnetic phases, it is required to use two reference temperature points [96].

The analysis of the universal scale demonstrates magnetic homogeneity. This approach should remove the dependency of the set of curves $\Delta S_{\rm M}$(H, T) on both temperature and field so that all curves treated using the same scaling procedure will collapse on a common universal curve. A lack of success in achieving this universal collapse can be explained by a magnetic inhomogeneity in the material [96]. As described above, we use detailed statistical analysis to determine the magnetic homogeneity in the material and the order of magnetic transition.

After rescaling temperature and choosing a=0.5, Fig. 13 shows that the normalized entropy change for all applied magnetic fields collapses in a single universal curve. This suggests that $Pr_{1.64}Sm_{0.36}Fe_{17}$ is magnetically homogeneous undergoes a second-order magnetic transition phase around T_C=299 K.

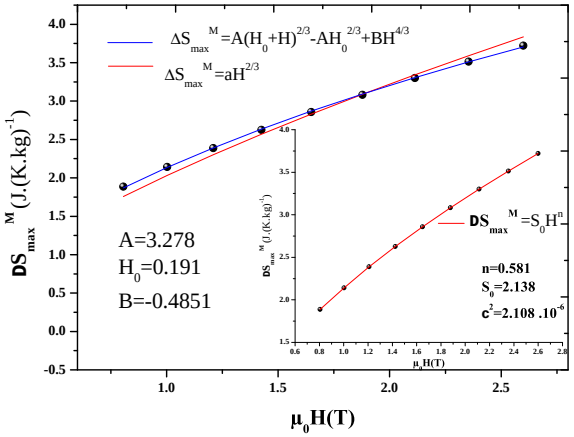

Figure 16. Field dependence of magnetic entropy change at T_C for $Pr_{1.64}Sm_{0.36}Fe_{17}$ sample.

Fig. 13 clearly shows that magnetic entropy change of $Pr_{1.64}Sm_{0.36}Fe_{17}$ sample reach its maximum around Curie temperature. The maximum of magnetic entropy change depends strongly on the applied magnetic field. A nonlinear relation can be expected between ΔS_M^{max} and $\mu_0 H$ as follows:

$$\Delta S_M^{max} \sim \mu_0 H^n$$

where n=2/3 in the case of mean field model [97]. For real ferromagnetic material the previous relation was rectified by Lyubina *et al* [98]. It was modified as follow:

$$\Delta S_M^{max} = A(\mu_0 H + H_0)^n - AH_0^{2/3} + B(\mu_0 H)^{4/3}$$

Where A and B are intrinsic parameters of the material and H_0 is a measure of homogeneity of the compound. Fig. 16 shows ΔS_M^{max} vs $\mu_0 H$ and fit parameters. One can easily notice that the fit of the experimental data with $\Delta S_M^{max} = a(\mu_0 H)^{2/3}$ equation is failed, on the other hand, $\Delta S_M^{max} = A(\mu_0 H + H_0)^n - AH_0^{2/3} + B(\mu_0 H)^{4/3}$ equation has clearly been in good agreement with the MCE behaviour of $Pr_{1.64}Sm_{0.36}Fe_{17}$ sample, similar behavior was observed in Ref. [86, 99]. It confirms the second-order nature of his magnetic transition, as demonstrated above by Both the Landau model and Arrott plot. The experimental data follow $\Delta S_M^{max} = a(\mu_0 H)^n$ equation with the local exponent n equals to 0.581. The obtained values of n are slightly deviated from the typical value of $n = 2/3$ within the mean-field model [100]. This deviation justifies the invalidity of the mean-field model for our sample. For materials that exhibit a second-order magnetic transition phase, it has been demonstrated in previous work that magnetic entropy change can be expressed as $\Delta S_M^{max} \propto H^{n(T,H)}$ [101]. The exponent n can be locally determined using the following relation:

$$n(T, H) = \frac{dln\Delta_M}{dlnH}$$

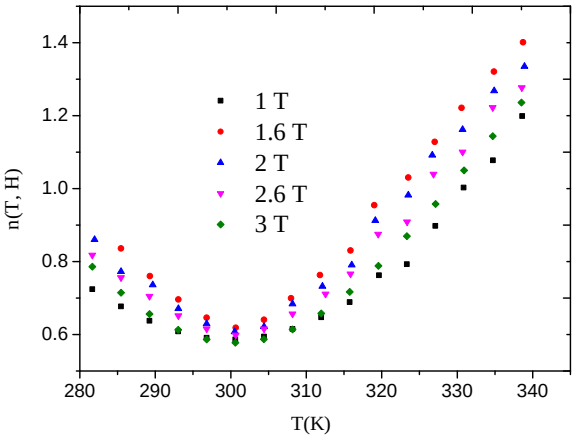

Figure 17. Temperature dependence of the local exponent n at different magnetic fields from 1 to 3 T for $Pr_{1.64}Sm_{0.36}Fe_{17}$ sample.

In the paramagnetic state n$\longrightarrow$2 when T $\gg T_C$, in the ferromagnetic state n$\longrightarrow$1 when T $\ll T_C$ and around magnetic phase transition (T$\longrightarrow T_C$) n(T_C)=1+(β − 1)/($\beta + \gamma$). Previous works have reported that the exponent n depends on the temperature and the applied magnetic field; it is known that for materials with a single magnetic phase, n is field independent at Curie

temperature. Nevertheless, in the case of materials that present multi magnetic phase, n is field-dependent at any temperature [102]. Fig. 17 shows the variation of the local exponent n with the temperature at several magnetic fields calculated using the logarithmic derivative of ΔS_M with an applied magnetic field. Fig. 17 shows that the exponent n is field-dependent below and above T_C, in contrast, at T=T_C is almost constant, unlike the behaviour observed for multiphase systems where n is field-dependent in Ref. [103, 104]. The Rietveld refinement of $Pr_{1.64}Sm_{0.36}Fe_{17}$ sample, a thermal derivative of magnetization, the universal curve of magnetic entropy change and the behaviour of n exponent at Curie temperature indicates that our sample presents a single-phase and a single magnetic phase transition. For different magnetic field $n \sim 0.58$, is deviated from the n value of the mean-field model but is consistent with the value calculated from $n(T_C)$ expression using the values of β and γ of the Ising model ($\beta = 0.325$, $\gamma = 1.241$), this suggests that the mean-field model is not the appropriate model to describe the magnetic phase transition in our sample.

IV. CONCLUSION

The structural, magnetic, and magnetocaloric properties have been studied for the intermetallic (Pr, Sm)$_2$Fe$_{17}$ compound. X-ray diffraction at room temperature shows that this compound crystallizes in the rhombohedral Th_2Zn_{17} type structure. Rietveld refinement shows that the cell parameters decrease when the Sm replaces the Pr. After the substitution of Pr by the Sm T_C increases from 285 to 299 K. This increase of T_C is mainly due to the de Gennes factor. The study of the phase transition according to the Landau model proves that $Pr_{1.64}Sm_{0.36}Fe_{17}$ exhibits a second-order transition phase. The magnetic entropy change, relative cooling power and TEC, were calculated. The value of T_C, which is close to the room temperature and a large temperature range with a quasi constant ΔS_{M} value, consequently the studied compound exhibits a good magnetocaloric effect.

ACKNOWLEDGMENTS

This work was supported by the National Center for Scientific Research (CNRS), France, and by the Ministry of Higher Education and Scientific Research Of Tunisia "(LMOP LR99ES17) Laboratory, Tunisia.

[1] J. X. Zhang, L. Bessais, C. Djega Mariadassou, E. Leroy, and A. Percheron Guegan. *Appl. Phys. Lett.*, 80(11):1960–1962, 2002.

[2] M. Murakami. *J. Appl. Phys.*, 101(9):09C522, 2007.

[3] J. F. Liu, P. Vora, M. H. Walmer, E. Kottcamp, S. A. Bauser, A. Higgins, and S. Liu. *J. Appl. Phys.*, 97(10):10H101, 2005.

[4] K. J. Strnat. *Cobalt, 36 (1967) 133-143*, 1967.

[5] R. Fersi, N. Mliki, L. Bessais, R. Guetari, V. Russier, and M. Cabie. *J. Alloys Compd.*, 522:14–18, 2012.

[6] W. Bouzidi, N. Mliki, and L. Bessais. *J. Magn. Magn. Mater.*, 441:566–571, 2017.

[7] A. M. Tishin and Y. I. Spichkin. *Institute of Physics Publishing, Bristol and Philadelphia*, 2003.

[8] S. Yu Dankov, A. M. Tishin V. V. Ivtchenko, K. A. Jr. Gschneidner, and V. K. Pecharsky. *Adv. Cryog. Eng.*, 46:397, 2000.

[9] G. Calestani, N. Magnani, A. Paoluzi, L. Pareti, and C. Rizzoli. *Phys. Rev. B*, 68(5):054424, 2003.

[10] A. M. Tishin and Y. I. Spichkin. Institute of Physics Publishing, Dirac House Temple Back, Bristol UK, 2003.

[11] K. Mandal, A. Yan, P. Kershl, A. Handstein, O. Gutfleisch, and K. H. Muller. *J. Phys. D*, 37:2628, 2004.

[12] H. Chen, Y. Zhang, J. Han, H. Du, Ch. Wang, and Y. Yang. *J. Magn. Magn. Mater.*, 320:1382–1384, 2008.

[13] P. Gorria, P. Alvarez, J. Sanchez Marcos, J. Sanchez-Llamazares, M. J. Perez, and J. A. Blanco. *Acta Mater.*, 57:1724–1733, 2009.

[14] S. Dan, S. Mukherjee, C. Mazumdar, and R. Ranganathan. *RSC Adv*, 6(97):94809–94814, 2016.

[15] S. Dan, S. Mukherjee, C. Mazumdar, and R. Ranganathan. *J. Phys. Chem. Solids*, 115:92–96, 2018.

[16] M. Saidi, K. Nouri, S. Walha, E. Dhahri, A. Kabadou, M. Jemmali, and L. Bessais. *J. Electron. Mater.*, 48:2242–2253, 2019.

[17] S. Dan, S. Mukherjee, C. Mazumdar, and R. Ranganathan. *J. Phys. Chem. Solids*, 21(5):2628–2638, 2019.

[18] W. Bouzidi, K. Nouri, T. Bartoli, R. Sedek, H. Lassri, J. Moscovici, and L. Bessais. *J. Magn. Magn. Mater.*, 497:166018, 2020.

[19] Y. Cao, K. Lin, Z. Liu, J. Hu, C-W. Wang, E. Tereshina-Chitrova, K. Kato, Q. Li, J. Deng, J. Chen, et al. *Inorg. Chem.*, 59(16):11228–11232, 2020.

[20] X. C. Kou, F. R. de Boer, R. Grössinger, G. Wiesinger, H. Suzuki, H. Kitazawa, T. Takamasu, and G. Kido. *J. Magn. Magn. Mater.*, 177-181:1002–1007, 1998.

[21] O. Isnard, S. Miraglia, D. Fruchart, E. Akiba, and K. Nomura. *J. Alloys Compd.*, 257:150–155, 1997.

[22] K. Mori, A. E. Clark, and O. D. McMasters. *J. Magn. Magn. Mater.*, 31-34:855–856, 1983.

[23] H. Sun, J. M. D Coey, Y. Otani, and D. P. F. Hurley. *J. Phys. Condens. Matter*, 2:6465–6470, 1990.

[24] G. J. Long, O. A. Pringle, F. Grandjean, W. B. Yelon, and K. H. J. Buschow. *J. Appl. Phys.*, 73:6050, 1993.

[25] Y. Zeng, Z. H. Lu, N. Tang, X. W. Li, R. W. Zhao, and F. M. Yang. *J. Magn. Magn. Mater.*, 139:11–18, 1995.

[26] S. A. Nikitin, G. Myalikgulyev, K. A. Asatryan A. M. Tishin, M. P. Annaorazov, and A. L. Tyurin. *Phys. Lett. A*, 148:363–366, 1990.

[27] V. K. Pecharsky and K. A. Gschneidner. *Phys. Rev. Lett.*, 78:4494, 1997.

[28] H. Wada, S. Tomekawa, and M. Shiga. *Cryogenics*, 39:915–919, 1999.

[29] H. Wada and Y. Tanabe. *Appl. Phys. Lett.*, 79:3302–3304, 2001.

[30] K. A. Gschneidner, V. K. Pecharsky, and A. O. Tsokol. *Rep. Prog. Phys.* , 68:1479, 2005.

[31] A. Fujita. *J. Appl. Phys.*, 127:123902, 2020.

[32] W. J. Lai, X. M. You, I Dugulan, B. W. Huang, J. Liu, M. Maschek, L. van Eijck, N. Dijk, and E. Bruck. *J. Alloys Compd.*, 821:153451, 2020.

[33] V. K. Pecharsky and K. A. Gschneidner. *J. Magn. Magn. Mater.*, 167:L179, 1997.

[34] K. A. Gschneidner, V. K. Pecharsky, E. Brück, H. G. M. Duijin, and E. M. Levin. *Phys. Rev. Lett.*, 85:4190, 2000.

[35] H. Tang, V. K. Pecharsky, G. D. Samolyuk, M. Zou, K. A. Gschneidner, V. P. Antropov, D. L. Schlagel, and T. A. Lograsso. *Phys. Rev. Lett.*, 93:237203, 2004.

[36] S. Fujieda, A. Fujita, and K. Fukamichi. *Appl. Phys. Lett.*, 81:811276–8, 2002.

[37] A. Fujita, S. Fujieda, and K. Fukamichi. *J. Magn. Magn. Mater.*, 310:e1006–e1007, 2007.

[38] A. Fujita, S. Fujieda, and K. Fukamichi. *J. Magn. Magn. Mater.*, 321:3553–3558, 2009.

[39] M. Phejar, V. Paul-Boncour, and L. Bessais. *Intermetallics*, 18:2301, 2010.

[40] A. Boutahar, M. Phejar, V. Paul-Boncour, L. Bessais, and H. Lassri. *J. Supercond. Nov. Magn.*, 27:1795–1800, 2014.

[41] M. Phejar, V. Paul-Boncour, and L. Bessais. *J. Solid State Chem.*, 223:95–102, 2016.

[42] O. Tegus, B. Fuquan, W. Dagula, L. Zhang, E. Brück, P. Z. Si, F. R. de Boer, and K. H. J. Buschow. *J. Alloys Compd.*, 396:6–9, 2005.

[43] A. Bartok, M. Kustov, L. F. Cohen, A. Pasko, K. Zehani, L. Bessais, F. Mazaleyrat, and M. LoBue. *J. Magn. Magn. Mater.*, 400:333–338, 2016.

[44] A. Bartok, M. Kuepferling, C. Curcio, V. Basso, A. Pasko, K. Zehani, L. Bessais, F. Mazaleyrat, and M. Lobue. *Refrigeration Science and Technology*, pages 119–122. 2016.

[45] A. Pasko, A. Bartok, K. Zehani, L. Bessais, F. Mazaleyrat, and M. LoBue. *AIP Advances*, 6:056204, 2016.

[46] A. R. Dinesen, S. Linderoth, and S. Morup. *J. Phys. Condens. Matter*, 17:6257, 2005.

[47] Z. Wei, A. Chak-Tong, and D. You-Wei. *Chin. Phys. B*, 22:057501, 2013.

[48] H. Felhi, M. Smari, A. Bojorek, K. Nouri, E. Dhahri, and L. Bessais. *Prog. Nat. Sci.*, 29:198–209, 2019.

[49] N. Ameur, F. Elleuch, M. Triki, E. Dhahri, L. Bessais, and E. K. Hlil. *Solid State Comm.* , 289:30–37, 2019.

[50] L. Bessais, E. Dorolti, and C. Djega-Mariadassou. *Appl. Phys. Lett.*, 87, 2005.

[51] N. Hosni, K. Zehani, T. Bartoli, L. Bessais, and H. Maghraoui-Meherzi. *J. Alloys Compd.*, 694:1295–1301, 2017.

[52] S. Khazzan, N. Mliki, L. Bessais, and C. Djega-Mariadassou. *J. Magn. Magn. Mater.*, 322(2):224–229, 2010.

[53] R. Bensalem, W. Tebib, S. Alleg, J. J. Sunol, L. Bessais, and J. M. Greneche. *J. Alloys Compd.*, 471:24–27, 2009.

[54] K. Zehani, R. Bez, A. Boutahar, EK Hlil, H. Lassri, J. Moscovici, N. Mliki, and L. Bessais. *J. Alloys Compd.*, 591:58–64, 2014.

[55] A. Hamrita, Y. Slimani, M. K. Ben Salem, E. Hannachi, L. Bessais, F. Ben Azzouz, and M. Ben Salem. *Ceram. int.*, 40:1461–1470, 2014.

[56] H. Rietveld. *Acta Crystallogr.*, 22:151, 1967.

[57] H. Rietveld. *J. Appl. Crystallogr.*, 2:65, 1969.

[58] J. Rodriguez-Carvajal. *Physica B* , 192:55, 1993.

[59] J. Rodriguez-Carvajal, M. T. Fernandez-Diaz, and J. L. Martinez. *J. Phys.* , 81:210, 2000.

[60] L.Bessais, S. Sab, C. Djega-Mariadassou, NH. Dan, and NX. Phuc. *Phys Rev B*, 70(13):134401, 2004.

[61] C. Djega-Mariadassou, L. Bessais, A. Nandra, and E. Burzo. *Phys. Rev. B*, 68:24406, 2003.

[62] L. Bessais, S. Sab, C. Djega-Mariadassou, N. H. Dan, and N. X. Phuc. *Phys. Rev. B*, 70:134401, 2004.

[63] K. Younsi, V. Russier, and L. Bessais. *J. Appl. Phys.*, 107:083916, 2010.

[64] Qu. Johnson, D. H. Wood, G. S. Smith, and A. E. Ray. *Acta Crystallogr. B Struct. Cryst. Cryst. Chem*, 24(2):274–276, 1968.

[65] R. Guetari, R. Bez, C. B. Cizmas, N. Mliki, and L. Bessais. *J. Alloys Compd.*, 579:156–159, 2013.

[66] S. Khazzan, N. Mliki, and L. Bessais. *J. Appl. Phys.*, 105:103904, 2009.

[67] C. Romero-Muniz, J. J. Ipus, J.S. Blázquez, V. Franco, and A. Conde. *Appl. Phys. Lett.*, 104(25):252405, 2014.

[68] A. K. Pramanik and A. Banerjee. *J. Phys: Condens. Matter*, 20(27):275207, 2008.

[69] M. Vatanparast, Y.T. Shao, M Rajpalke, B. Fimland, T. Reenaas, E. Holmestad, P. Vullum, and J.M. Zuo. *Ultramicroscopy*, page 113299, 2021.

[70] I. V. Bodnar, I.A. Victorov, O.V Alita, V.V. Khoroshko, and E. Arushanov. *Solid State Sci.*, 113:106550, 2021.

[71] L. Vegard. *Zeitschrift für Physik*, 5(1):17–26, 1921.

[72] R. Guetari, R. Bez, A. Belhadj, K. Zehani, A. Bezergheanu, N. Mliki, L. Bessais, and C. B. Cizmas. *J. Alloys Compd.*, 588:64–69, 2014.

[73] K. H. J. Buschow. volume 4, page 44. North-Holland, Amsterdam, north-holland, amsterdam edition, 1988.

[74] L. Bessais, C. Djega-Mariadassou, A. Nandra, M. D. Appay, and E. Burzo. *Phys. Rev. B*, 69:64402, 2004.

[75] K. Inoue, Y. Nakamura, A. V. Tsvyashchenko, and L. Fomichiva. *J. Phys. Soc. Jpn.*, 64(6):2175–2182, 1995.

[76] M. R. Ibarra J. L. Wang, C. Marquina and G. H. Wu. *Phys. Rev. B*, 73(9):094436, 2006.

[77] R. M. Bozorth. *J. Appl. Phys.*, 38(3):1366–1371, 1967.

[78] H. R. Kirchmayr and C. A. Poldy. *J. Magn. Magn. Mater.*, 8(1):1–42, 1978.

[79] Z. W. Li and X. A. H. Morrish. *Phys. Rev. B*, 55:3670–3676, 1997.

[80] M. Foldeaki, R. Chahine, and T. K. Bose. *J. Appl. Phys.*, 77:3528, 1995.

[81] P. Alvarez, P. Gorria, V. Franco, J. Sanchez Marcos, M. J. Perez, J. Sanchez-Llamazares, I. Puente-Orench, and J. Blanco. *J. Phys. Condens. Matter*, 22:216005, 2010.

[82] V. K. Pecharsky and K. A. Gschneidner Jr. *Phys. Rev. Lett.*, 78(23):4494, 1997.

[83] P. Kumar, KG. Suresh, AK. Nigam, and O. Gutfleisch. *J. Phys. D J PHYS D APPL PHYS*, 41(24):245006, 2008.

[84] S K. Tripathya, K G. Suresha, and A K. Nigam. *J. Magn.Magn. Mater. 306 24*, 2006.

[85] Z. Jun-Ding, S. Bao-Gen, , and S. Ji-Rong. *Chin. Phys. Soc.*, 16(12):3843, 2007.

[86] A. Sakka, R. M'nassri, MM. Nofal, S. Mahjoub, W. Cheikhrouhou-Koubaa, N. Chniba-Boudjada, M. Oumezzine, and A. Cheikhrouhou. *J. Magn. Magn. Mater.*, 514:167158, 2020.

[87] L. Su, X.Q. Zhang, Q.Y. Dong, H. T. Yangand S. H. Li, and Z. H. Cheng. *Ceram. Int*, 47(13):18286–18294, 2021.

[88] S. Choura-Maatar, M.M. Nofal, R. Mnassri, W. Cheikhrouhou Koubaa, N. Chniba Boudjada, and A. Cheikhrouhou. *J. Mater. Sci.: Mater. Electron.*, 31:1634–1645, 2020.

[89] D. Mazumdar and I. Das. *J. Appl. Phys.*, 129(6):063901, 2021.

[90] L. D. Griffith, Y. Mudryk, J. Slaughter, and V. K. Pecharsky. *Journal of Applied Physics*, 123(3):034902, 2018.

[91] R. C. Zhang, M. F. Qian, X. X. Zhang, F. X. Qin, L. S. Wei, D. W. Xing, X. P. Cui, J. F. Sun, L. Geng, and H. X. Peng. *J. Magn. Magn. Mater.*, 428:464–468, 2017.

[92] G. J. Liu, J. R. Sun, J. Shen, B. Gao, H. W. Zhang, F. X. Hu, and B. G. Shen. *Appl. Phys. Lett.*, 90(3):032507, 2007.

[93] M. Balli, D. Fruchart, D. Gignoux, and R. Zach. *Appl. Phys. Lett.*, 95(7):072509, 2009.

[94] A. Das and A. K. Majumdar. *J. Magn. Magn. Mater.*, 128(1-2):47–57, 1993.

[95] V. Franco, J. S. Blazquez, and A. Conde. *Appl. Phys. Lett*, 89:222512, 2006.

[96] V. Franco and A. Conde. *Int. J. Refrig.*, 33(3):465–473, 2010.

[97] M. Seeger, S.N. Kaul, K. Kronmüller, and R. Reisser. *Phys. Rev. B*, 51(18):12585, 1995.

[98] J. Lyubina, M.D. Kuzmin, K. Nenkov, O. Gutfleisch, M. Richter, D.L. Schlagel, T.A. Lograsso, Jr. Gschneidner, and A. Karl. *Phys Rev B*, 83(1):012403, 2011.

[99] S. Chandra, A. Biswas, S. Datta, B. Ghosh, V. Siruguri, AK. Raychaudhuri, MH. Phan, and H. Srikanth. *J. Condens. Matter Phys.*, 24(36):366004, 2012.

[100] H. Oesterreicher and F.T. Parker. *J. Appl. Phys.*, 55(12):4334–4338, 1984.

[101] J. S. Blazquez V. Franco and A. Conde. *Appl. Phys. Lett*, 89:222512, 2006.

[102] V. Franco, J.S. Blázquez, B. Ingale, and A. Conde. *Annu. Rev. Mater. Res*, 42, 2012.

[103] J.J. Ipus, J.S. Blázquez, V. Franco, A. Conde, and L.F. Kiss. *Int. J. Appl. Phys*, 105(12):123922, 2009.

[104] H. Ben Khlifa, R. M'nassri, W. Cheikhrouhou-Koubaa, G. Schmerber, and A. Cheikhrouhou. *J. Magn. Magn. Mater.*, 466:7–16, 2018.